Numerical simulations of classical problems in two-dimensional (non) linear second gradient elasticity

Ugo Andreaus (a), Francesco dell'Isola (a), Ivan Giorgio (a), Luca Placidi (b), Tomasz Lekszycki (c), Nicola Luigi Rizzi (d)

(a) Università di Roma La Sapienza. Department of structural and geotechnical engineering.

(b) International Telematic University Uninettuno, C.so Vittorio Emanuele II, 39 00186 Roma. Corresponding author.

(c) Warsaw University of Technology, Faculty of Engineering Production Warsaw.

(d) Dipartimento di Architettura, Università degli studi Roma Tre, Rome, Italy.

Abstract

A two-dimensional solid consisting of a linear elastic isotropic material is considered in this paper. The strain energy is expressed as a function of the strain and of the gradient of strain. The balance equations and the boundary conditions have been derived and numerically simulated for those classical problems for which an analytical solution is available in the literature. Numerical simulations have been developed with a commercial code and a perfect overlap between the results and the analytical solution has been found. The role of external edge double forces and external wedge forces has also been analyzed. We investigate a mesh-size independency of second gradient numerical solutions with respect to the classical first gradient one. The necessity of a second gradient modelling is finally shown. Thus, we analyse a non-linear anisotropic problem, for which experimental evidence of internal boundary layer is shown and we prove that this can be related to the second gradient modelling.

Keywords: Second gradient, Elasticity, Variational approach, Isotropy, Anisotropy, Numerical solution, Two-dimensional problems

Email address: `luca.placidi@uninettunouniversity.net` (Ugo Andreaus (a), Francesco dell'Isola (a), Ivan Giorgio (a), Luca Placidi (b), Tomasz Lekszycki (c), Nicola Luigi Rizzi (d))

1. Introduction

The introduction of higher order gradients of the strain into the constitutive law for the internal energy leads to a partial differential equation of higher orders and the Galerkin method requires a higher regularity of the interpolation scheme, see e.g. [14]. The reason of introducing higher-order gradient theories is based on different points of view, see e.g. [6, 7, 8, 9]. The first example is referred to the case related to strongly localized deformation features [3, 21, 59, 60, 65] and references therein. In such cases, it is reasonable to complement the displacement field with some additional kinematical descriptors [34, 35, 36, 55, 56, 58, 63], which leads to the so-called micromorphic models, see also [38, 43, 44, 51]. Another possibility is to consider higher order gradient theories, in which the deformation energy depends on second and/or higher gradients of the displacement [27, 31, 42]. This is done in the literature for both monophasic systems (see [12, 64], in which continuous systems are investigated, and [2, 70] for cases of lattice/woven structures) and for bi-phasic (see e.g. [10, 26, 49, 69]) or granular materials [50, 74]. The second example is referred to the fact that, unlike classical Cauchy continua, second and higher order continua can respond to concentrated forces and generalized contact actions (see e.g. in [17, 23]). It is worth to be noted that it is also possible to conceive a framework in classical elasticity (see, e.g., [16, 47] and references therein) in which concentrated forces are possible. However, with a greater theoretical and numerical efforts. The third example is becoming increasingly important for practical and applicative reasons in the last years, as the novelties in manufacturing procedures (due to, e.g., 3D printing, self assembly etc.) are making possible the realization of a much wider class of new architectured materials [24, 46]. In these cases, the deficiencies of classical approaches when the material behaviour exhibits size-scale effects is investigated in [66, 67, 68], and in [52] a novel invariance requirement (micro-randomness) in addition to isotropy is formulated, which implies conformal invariance of the curvature. In general, new theories are put into place when existing theories prove to be inadequate to describe some observed phenomenon. Such new theories however have to lead to well posed problems in the sense that the governing equations and boundary conditions lead to solvable problems. The papers [2, 45, 57] already proved that the problems we study here is indeed well-posed.

A survey of variational principles, which form the basis for computational methods in both continuum mechanics and multi-rigid body dynamics is presented in [5] and numerical investigation of structures of the type considered also requires special attention and the development of novel techniques [4, 15, 18, 19, 20, 37, 39] or the proper employment of the existing ones (see for instance [71], where Galerkin Boundary Element Method is used to address a class of strain gradient elastic materials). The objective of the contribution [41] is to formulate a geometrically nonlinear theory of higher-gradient elasticity accounting for boundary (surface and curve) energies. To reduce the computational costs and avoid the macroscopic grid sensitivity, an adaptive multiscale technique is developed for strain localization analysis of periodic lattice truss materials in [79]. In [75] a general finite element discretization of micromorphic Mindlin's elasticity is presented. The behaviour of all elements is also examined at the limiting case of strain gradient elasticity. The numerical solution of second gradient elasticity equations with a displacement-based finite element method requires the use of C1-continuous elements, that motivates the implementation of the concept of isogeometric analysis in [32]. In [54] a new C1 hexahedral element which is the first three-dimensional C1 element ever constructed and give excellent rates of convergence in a benchmark (without edge forces) boundary value problem of gradient elasticity. In [53] a methodology by which C1 elements, such as the TUBA 3 element proposed by Argyris et al. [11], can be constructed is presented. This kind of elements are largely present in the literature of strain gradient elasticity [1, 22, 33, 76, 77, 78].

From a general point of view a comparison between analytical and numerical solution is needed to check the quality of the used code. In other words, it means that the code has good performances and there is a degree of reliability to be assigned to it. In this paper a two-dimensional solid consisting of a linear elastic isotropic material is considered. The strain energy is expressed as a function of the strain and of the gradient of strain. The aim of the paper is to present the possibility to numerically simulate general strain gradient elasticity by the use of a commercial code that includes the Argyris shape functions. This is done with the use of benchmark boundary value problem for which an analytical solution exist. We remark that in such a 2-dimensional benchmark boundary value problem wedge forces are present. We remark a perfect overlap between the numerical results and the analytical solution of the benchmark classical boundary value problem. The role of external edge double forces and external wedge forces has also been analyzed. We also investigate a mesh-size independency of second gradient numerical solutions with respect to the classical first gradient one. Finally, we show an experimental evidence of the necessity of second gradient modelling. We show the experimental results [25] of a bias test on a pantographic structure. In particular, we show that the boundary layer experimentally observed can be numerically achieved by a non-null second gradient constitutive coefficient and the largeness of such a boundary layer can be used to identify such a second gradient parameter. For a better representation of the state of the art of material identification of second gradient coefficients the reader is invited to see [13, 61, 62].

2. Formulation of the problem

2.1. The general case

The coordinates X, in the reference configuration, are those of the 2-dimensional body$\mathcal{B}$. The internal energy density functional $U(G,\nabla G)$ depends not only on the strain $G=\left(F^T F - I\right)/2$ but also on its gradient ∇G, where $F=\nabla\chi$, χ is the placement function. In Mindlin [48] a general form of the density of the strain energy functional of a linear isotropic second gradient elastic material is given, for the sake of simplicity, in indicial notation,

$$\begin{aligned} U(G,\nabla G) &= \frac{\lambda}{2}G_{ii}G_{jj}+\mu G_{ij}G_{ij}+ \\ &+4\alpha_1 G_{aa,b}G_{bc,c}+\alpha_2 G_{aa,b}G_{cc,b}+4\alpha_3 G_{ab,a}G_{cb,c}+2\alpha_4 G_{ab,c}G_{ab,c}+4\alpha_5 G_{ab,c}G_{ac,b}, \end{aligned} \tag{1}$$

where subscript j after comma indicates derivative with respect to X_j and a general rule for index notation is the following: the subscript-indeces of a symbol denoting a vector or a tensor quantity denote the components of that quantity. In the 2-dimensional case we have

$$\begin{aligned} U(G,\nabla G) = \tilde{U}(u) &= (\lambda+2\mu)\left(u_{1,1}^2+u_{2,2}^2\right)+\mu\left(u_{1,2}^2+u_{2,1}^2\right)+2\lambda u_{1,1}u_{2,2}+2\mu u_{1,2}u_{2,1} \\ &+\frac{1}{2}A\left(u_{1,22}^2+u_{2,11}^2\right)+\frac{1}{2}B\left(u_{1,11}^2+u_{2,22}^2\right)+C\left(u_{1,12}^2+u_{2,12}^2\right)+2D\left(u_{1,11}u_{2,12}+u_{2,22}u_{1,12}\right) \\ &+\frac{1}{2}(A+B-2C)\left(u_{1,11}u_{1,22}+u_{2,11}u_{2,22}\right)+(B-A-2D)\left(u_{1,12}u_{2,11}+u_{1,22}u_{2,12}\right), \end{aligned} \tag{2}$$

where

$$A = 2\alpha_3 + 2\alpha_4 + 2\alpha_5, \qquad B = 8\alpha_1 + 2\alpha_2 + 8\alpha_3 + 4\alpha_4 + 8\alpha_5. \tag{3}$$

$$C = 2\alpha_1 + \alpha_2 + \alpha_3 + 3\alpha_4 + 5\alpha_5, \qquad D = 3\alpha_1 + \alpha_2 + 2\alpha_3, \tag{4}$$

where u is the displacement field, λ and μ are the Lamè coefficients and α_i with $i = 1, 2, 3, 4, 5$ are the 5 second gradient constitutive parameters. Note that here we use the Lamè coefficients λ and μ to describe first-gradient, isotropic linear elasticity, but other choices could be made, e.g., the pair comprised of bulk modulus κ and shear modulus μ [28, 29, 30, 40, 72, 73], which is particularly convenient, e.g., when treating quasi-incompressibility.

In Mindlin [48], in order to have the positive definiteness of U, the following restrictions on the 7 constitutive parameters must be satisfied,

$$\mu > 0, \quad 3\lambda + 2\mu > 0, \quad -4\alpha_1 + 2\alpha_2 + 2\alpha_3 + 6\alpha_4 - 6\alpha_5 > 0, \quad \alpha_4 > \alpha_5, \quad \alpha_4 + 2\alpha_5 > 0 \tag{5}$$
$$4\alpha_1 + \alpha_2 + 4\alpha_3 + 2\alpha_4 + 4\alpha_5 > 0, \quad \alpha_1 + \alpha_2 < \alpha_3, \quad 4\alpha_1 - 2\alpha_2 - 2\alpha_3 - 3\alpha_4 + 3\alpha_5 > 0.$$

In the 2-dimensional case the positive definiteness of U is implied again by the classical 2-dimensional restrictions

$$\mu > 0, \quad \lambda + \mu > 0,$$

and by the positive definiteness of the following matrix

$$\begin{pmatrix} A & 0 & \frac{1}{2}(A+B-2C) & 0 & 0 & B-A-2D \\ 0 & A & 0 & \frac{1}{2}(A+B-2C) & B-A-2D & 0 \\ \frac{1}{2}(A+B-2C) & 0 & B & 0 & 0 & 2D \\ 0 & \frac{1}{2}(A+B-2C) & 0 & B & 2D & 0 \\ 0 & B-A-2D & 0 & 2D & 2C & 0 \\ B-A-2D & 0 & 2D & 0 & 0 & 2C \end{pmatrix}.$$

Keeping this in mind, a classical variational procedure gives the following system of partial differential equations $\forall X_i \in \mathcal{B}$,

$$u_{1,11}(\lambda+2\mu)+u_{1,22}\mu+u_{2,12}(\lambda+\mu)=$$
$$=u_{1,1111}B+u_{1,2222}A+u_{1,1122}(A+B)+(u_{2,1222}+u_{2,1112})(B-A)-b_1^{ext} \qquad (6)$$

$$u_{2,22}(\lambda+2\mu)+u_{2,11}\mu+u_{1,12}(\lambda+\mu)=$$
$$=u_{2,2222}B+u_{2,1111}A+u_{2,1122}(A+B)+(u_{1,1222}+u_{1,1112})(B-A)-b_2^{ext}, \qquad (7)$$

and boundary conditions given $\forall X_i \in \partial\mathcal{B}$ from the following duality conditions

$$\delta u_\alpha\left(t_\alpha-t_\alpha^{ext}\right)=0,\ \delta u_{\alpha,j}n_j\left(\tau_\alpha-\tau_\alpha^{ext}\right)=0,\ \int_{[\partial\partial\mathcal{B}]}\delta u_\alpha f_\alpha=\int_{[\partial\partial\mathcal{B}]}\delta u_\alpha f_\alpha^{ext}, \qquad (8)$$

where b_α^{ext}, t_α^{ext}, τ_α^{ext} and f_α^{ext} are the external actions: b_α^{ext} is the external force per unit area and is applied on the whole 2-dimensional domain $\mathcal{B}$; t_α^{ext} and τ_α^{ext} are the external force and double force (respectively) and are applied on (a part of) the one-dimensional boundary $\partial\mathcal{B}$ of the domain $\mathcal{B}$; and f_α^{ext} is the external concentrated force applied on the set of points belonging to the boundary of the boundary $[\partial\partial\mathcal{B}]$, so that the last integral can be also represented as the sum of the external works made by the concentrated forces acting on each vertex of the domain. In other words, if we define the boundary $\partial\mathcal{B}$ as the union of m regular parts Σ_c with $c=1,\ldots,m$ and $[\partial\partial\mathcal{B}]$ as the union of the corresponding m vertex-points $\mathcal{V}_c$ with $c=1,\ldots,m$,

$$\partial\mathcal{B}=\bigcup_{c=1}^m \Sigma_c, \qquad [\partial\partial\mathcal{B}]=\bigcup_{c=1}^m \mathcal{V}_c,$$

then the line and vertex-integrals of a generic field $g(X_i)$ are represented as follows,

$$\oint_{\partial\mathcal{B}} g(X_i)=\sum_{c=1}^m\int_{\Sigma_c} g(X_i), \quad \int_{[\partial\partial\mathcal{B}]} g(X_i)=\sum_{c=1}^m g(X_i^c) \qquad (9)$$

where X_i^c is the coordinate of the vertex $\mathcal{V}_c$. Moreover, the so called contact force t_α, contact double

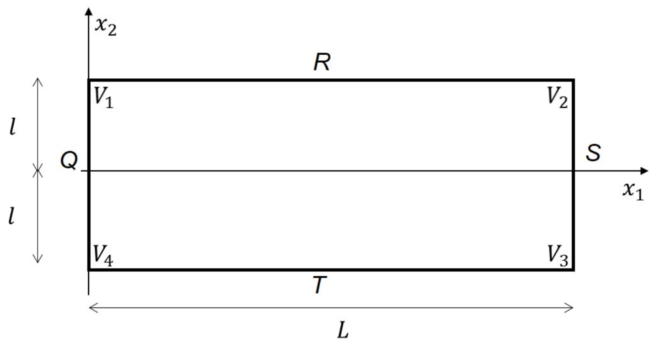

Figure 1: Picture of the 2-dimensional body$\mathcal{B}$.

force τ_α and contact wedge force f_α are defined,

$$t_\alpha = (S_{\alpha j} - T_{\alpha jh,h})\, n_j - P_{ka}\left(T_{\alpha hj} P_{ah} n_j\right)_{,k} \tag{10}$$

$$\tau_\alpha = T_{\alpha jk} n_j n_k \tag{11}$$

$$f_\alpha = T_{\alpha hk} V_{hk} \tag{12}$$

where n_i is the normal to the boundary $\partial\mathcal{B}$, P_{ij} is its tangential projector operator ($P_{ij} = \delta_{ij} - n_i n_j$), V is the vertex operator

$$V_{hj} = \nu_h^l n_j^l + \nu_h^r n_j^r,$$

where superscripts l and r refers (roughly speaking, left and right), respectively, to one and to the other sides that define a certain vertex-point $\mathcal{V}_c$; ν is the external tangent unit vector. Stress and hyper stresses are defined,

$$S_{ij} = \frac{\partial U}{\partial G_{ij}}, \qquad T_{ijh} = \frac{\partial U}{\partial G_{ij,h}}. \tag{13}$$

2.2. Rectangles

2.2.1. The general case of straight lines

In the case of boundaries $\partial\mathcal{B}$ composed of straight-lines, the contact force in (10), the contact double force in (11) and the contact wedge force (12) are

$$t_\alpha = S_{\alpha j} n_j - \left(T_{\alpha jh,h} + T_{\alpha hj,h}\right) n_j + T_{\alpha hj,k} n_h n_k n_j, \quad \tau_\alpha = T_{\alpha jk} n_j n_k, \quad f_\alpha = T_{\alpha ij} V_{ij}, \tag{14}$$

that, in terms of the displacement fields, yield,

$$\begin{aligned} t_\alpha &= \lambda u_{a,a} n_\alpha + \mu u_{\alpha,j} n_j + \mu u_{j,\alpha} n_j - u_{a,abb} n_\alpha \left(6\alpha_1 + 2\alpha_2 + 4\alpha_3\right) \\ &- u_{a,a\alpha k} n_k \left(6\alpha_1 + 2\alpha_2 + 4\alpha_3 + 2\alpha_4 + 8\alpha_5\right) - u_{\alpha,aak} n_k \left(2\alpha_3 + 4\alpha_4 + 6\alpha_5\right) \\ &- u_{k,\alpha aa} n_k \left(2\alpha_1 + 2\alpha_3 + 2\alpha_4 + 6\alpha_5\right) + u_{a,ajk} n_\alpha n_j n_k \left(4\alpha_1 + 2\alpha_2 + 2\alpha_3\right) \\ &+ u_{j,aak} n_\alpha n_j n_k \left(2\alpha_1 + 2\alpha_3\right) + u_{\alpha,abc} n_a n_b n_c \left(2\alpha_4 + 2\alpha_5\right) + u_{a,\alpha bc} n_a n_b n_c \left(2\alpha_4 + 6\alpha_5\right), \end{aligned} \tag{15}$$

$$\begin{aligned} \tau_\alpha &= u_{a,ab} n_\alpha n_b \left(4\alpha_1 + 2\alpha_2 + 2\alpha_3\right) + u_{a,bb} n_\alpha n_a \left(2\alpha_1 + 2\alpha_3\right) \\ &+ \left(2\alpha_1 + 2\alpha_3\right) u_{a,a\alpha} + u_{\alpha,ab} n_a n_b \left(2\alpha_4 + 2\alpha_5\right) + 2\alpha_3 u_{\alpha,aa} + u_{a,\alpha b} n_a n_b \left(2\alpha_4 + 6\alpha_5\right). \end{aligned} \tag{16}$$

We remark that the formulation expressed in (15) and (16) can also be used in the 3-dimensional case. This is the reason why (15) and (16) are expressed in terms of the 5 3-dimensional constitutive coefficients α_i with $i = 1, 2, 3, 4, 5$ and not in terms of the 4 2-dimensional constitutive coefficients A, B, C and D.

In Fig. 1 we represent the scheme of a rectangle with side-names Q, R, S and T and vertex-names V_1, V_2, V_3 and V_4.

2.2.2. Characterization of sides

The characterization of side S is done by setting $n_i = \delta_{i1}$. Thus, from (15) with $\alpha = 1, 2$, and from (16) with $\alpha = 1, 2$, we have

$$t_1 = t_1^S = u_{1,1}(\lambda + 2\mu) + u_{2,2}\lambda - Bu_{1,111} - 2Du_{2,222} - \frac{1}{2}(A + B + 2C)u_{1,122} - (B - A)u_{2,211}, \quad (17)$$
$$t_2 = t_2^S = \mu(u_{1,2} + u_{2,1}) - (B - A)u_{1,112} - (B - A - 2D)u_{1,222} - Au_{2,111} - \frac{1}{2}(A + B + 2C)u_{2,122}, \quad (18)$$
$$\tau_1 = \tau_1^S = Bu_{1,11} + \frac{1}{2}(A + B - 2C)u_{1,22} + 2Du_{2,12}, \quad (19)$$
$$\tau_2 = \tau_2^S = (B - A - 2D)u_{1,12} + Au_{2,11} + \frac{1}{2}(A + B - 2C)u_{2,22}. \quad (20)$$

The characterization of side Q is done by setting $n_i = -\delta_{i1}$. Thus, from (15) with $\alpha = 1, 2$, and from (16) with $\alpha = 1, 2$, we have

$$t_1 = t_1^Q = -u_{1,1}(\lambda + 2\mu) - u_{2,2}\lambda + Bu_{1,111} + 2Du_{2,222} + \frac{1}{2}(A + B + 2C)u_{1,122} + (B - A)u_{2,211}, \quad (21)$$
$$t_2 = t_2^Q = -\mu(u_{1,2} + u_{2,1}) + (B - A)u_{1,112} + (B - A - 2D)u_{1,222} + Au_{2,111} + \frac{1}{2}(A + B + 2C)u_{2,122}, \quad (22)$$
$$\tau_1 = \tau_1^Q = Bu_{1,11} + \frac{1}{2}(A + B - 2C)u_{1,22} + 2Du_{2,12}, \quad (23)$$
$$\tau_2 = \tau_2^Q = (B - A - 2D)u_{1,12} + Au_{2,11} + \frac{1}{2}(A + B - 2C)u_{2,22}. \quad (24)$$

We remark that t_1^Q in (21) and t_2^Q in (22) are the opposite of t_1^S in (17) and of t_2^S in (18), respectively, and that τ_1^Q in (23) and τ_2^Q in (24) are the same of τ_1^S in (19) and of τ_2^S in (20), respectively.

The characterization of side R is done by setting $n_i = \delta_{i2}$. Thus, from (15) with $\alpha = 1, 2$, and from (16) with $\alpha = 1, 2$, we have

$$t_1 = t_1^R = \mu(u_{1,2} + u_{2,1}) - (B - A)u_{2,122} - (B - A - 2D)u_{2,111} - Au_{1,222} - \frac{1}{2}(A + B + 2C)u_{1,112}, \quad (25)$$
$$t_2 = t_2^R = u_{2,2}(\lambda + 2\mu) + u_{1,1}\lambda - Bu_{2,222} - 2Du_{1,111} - \frac{1}{2}(A + B + 2C)u_{2,112} - (B - A)u_{1,122}, \quad (26)$$
$$\tau_1 = \tau_1^R = (B - A - 2D)u_{2,12} + Au_{1,22} + \frac{1}{2}(A + B - 2C)u_{1,11}, \quad (27)$$
$$\tau_2 = \tau_2^R = Bu_{2,22} + \frac{1}{2}(A + B - 2C)u_{2,11} + 2\mathrm{D}u_{1,12}. \quad (28)$$

We remark that, because of isotropy, t_1^R in (25) and t_2^R in (26) are the same of t_2^S in (18) and of t_1^S in (17), respectively, by changing the indexes 1 and 2. Besides, because of isotropy, τ_1^R in (27) and τ_2^R in (28) are the same of τ_2^S in (19) and of τ_1^S in (20), respectively, by changing the indexes 1 and 2.

Finally, the characterization of side T is done by setting $n_i = -\delta_{i2}$. Thus, from (15) with $\alpha = 1, 2$, and from (16) with $\alpha = 1, 2$, we have

$$t_1 = t_1^T = -\mu \left(u_{1,2} + u_{2,1}\right) + \left(B - A\right) u_{2,122} + \left(B - A - 2D\right) u_{2,111} + A u_{1,222} + \frac{1}{2} \left(A + B + 2C\right) u_{1,112}, \tag{29}$$

$$t_2 = t_2^T = -u_{2,2} \left(\lambda + 2\mu\right) - u_{1,1}\lambda + B u_{2,222} + 2D u_{1,111} + \frac{1}{2} \left(A + B + 2C\right) u_{2,112} + \left(B - A\right) u_{1,122}, \tag{30}$$

$$\tau_1 = \tau_1^T = \left(B - A - 2D\right) u_{2,12} + A u_{1,22} + \frac{1}{2} \left(A + B - 2C\right) u_{1,11}, \tag{31}$$

$$\tau_2 = \tau_2^T = B u_{2,22} + \frac{1}{2} \left(A + B - 2C\right) u_{2,11} + 2\mathrm{D} u_{1,12}. \tag{32}$$

We remark that t_1^T in (29) and t_2^T in (30) are the opposite of t_1^R in (25) and of t_2^R in (26), respectively, and that τ_1^T in (31) and τ_2^T in (32) are the same of τ_1^R in (27) and of τ_2^R in (28), respectively.

2.2.3. Characterization of vertices

The last equation of (8) is reduced, because of $(9)_2$ to

$$\begin{aligned} &\int_{[\partial\partial\mathcal{B}]} \delta u_\alpha \left(f_\alpha - f_\alpha^{ext}\right) = \\ &= \left[\delta u_\alpha \left(T_{\alpha ij} V_{ij} - f_\alpha^{ext}\right)\right]_{\mathcal{V}_1} + \left[\delta u_\alpha \left(T_{\alpha ij} V_{ij} - f_\alpha^{ext}\right)\right]_{\mathcal{V}_2} \\ &+ \left[\delta u_\alpha \left(T_{\alpha ij} V_{ij} - f_\alpha^{ext}\right)\right]_{\mathcal{V}_3} + \left[\delta u_\alpha \left(T_{\alpha ij} V_{ij} - f_\alpha^{ext}\right)\right]_{\mathcal{V}_4}, \end{aligned} \tag{33}$$

For vertex $\mathcal{V}_1$ the side A has $n_j = -\delta_{1j}$ and $\nu_i = \delta_{i2}$ and the side B has $n_j = \delta_{2j}$ and $\nu_i = -\delta_{i1}$ so that

$$\left[V_{ij}\right]_{\mathcal{V}_1} = \left[\nu_i^l n_j^l + \nu_i^r n_j^r\right]_{\mathcal{V}_1} = -\delta_{i2}\delta_{1j} - \delta_{i1}\delta_{2j}.$$

For vertex $\mathcal{V}_2$ the side B has $n_j = \delta_{2j}$ and $\nu_i = \delta_{i1}$ and the side C has $n_j = \delta_{1j}$ and $\nu_i = \delta_{i2}$ so that

$$[V_{ij}]_{\mathcal{V}_2} = \left[\nu_i^l n_j^l + \nu_i^r n_j^r\right]_{\mathcal{V}_2} = \delta_{i1}\delta_{2j} + \delta_{i2}\delta_{1j}.$$

For vertex $\mathcal{V}_3$ the side C has $n_j = \delta_{1j}$ and $\nu_i = -\delta_{i2}$ and the side D has $n_j = -\delta_{2j}$ and $\nu_i = \delta_{i1}$ so that

$$[V_{ij}]_{\mathcal{V}_3} = \left[\nu_i^l n_j^l + \nu_i^r n_j^r\right]_{\mathcal{V}_3} = -\delta_{i2}\delta_{1j} - \delta_{i1}\delta_{2j}.$$

For vertex $\mathcal{V}_4$ the side D has $n_j = -\delta_{2j}$ and $\nu_i = -\delta_{i1}$ and the side A has $n_j = -\delta_{1j}$ and $\nu_i = -\delta_{i2}$ so that

$$[V_{ij}]_{\mathcal{V}_4} = \left[\nu_i^l n_j^l + \nu_i^r n_j^r\right]_{\mathcal{V}_4} = \delta_{i1}\delta_{2j} + \delta_{i2}\delta_{1j}.$$

Thus, finally, the (33) yields

$$\int_{[\partial\partial\mathcal{B}]} \delta u_\alpha \left(f_\alpha - f_\alpha^{ext}\right) = \left[\delta u_\alpha \left(-T_{\alpha 21} - T_{\alpha 12} - f_\alpha^{ext}\right)\right]_{\mathcal{V}_1} + \left[\delta u_\alpha \left(T_{\alpha 12} + T_{\alpha 21} - f_\alpha^{ext}\right)\right]_{\mathcal{V}_2} \quad (34)$$

$$+ \left[\delta u_\alpha \left(-T_{\alpha 21} - T_{\alpha 12} - f_\alpha^{ext}\right)\right]_{\mathcal{V}_3} + \left[\delta u_\alpha \left(T_{\alpha 12} + T_{\alpha 21} - f_\alpha^{ext}\right)\right]_{\mathcal{V}_4},$$

where $T_{\alpha 12} + T_{\alpha 21}$, in terms of the displacement field, it is for $\alpha = 1$

$$T_{112} + T_{121} = 2Cu_{1,12} + (B - A - 2D)\, u_{2,11} + 2Du_{2,22}, \quad (35)$$

and for $\alpha = 2$,

$$T_{212} + T_{221} = 2Cu_{2,12} + (B - A - 2D)\, u_{1,22} + 2Du_{1,11}. \quad (36)$$

3. Numerical simulations

Numerical data for the simulations that will be presented in this paper are here shown (see Fig. 1)

$$L = 2m,\ l = 1m,\ \mu = 10MPa\,m,\ \lambda = 15MPa\,m,\ \rho = 10^5 Kg/m^2\ E = \frac{\mu\,(3\lambda + 2\mu)}{\lambda + \mu} = 26MPa\,m, \quad (37)$$

$$\alpha_1 = El_m^2, \quad \alpha_2 = El_m^2, \quad \alpha_3 = 2El_m^2, \quad \alpha_4 = El_m^2, \quad \alpha_5 = \frac{1}{2}El_m^2, \quad l_m = 10cm, \quad (38)$$

and therefore

$$A = 7El_m^2, \qquad B = 34El_m^2, \qquad C = \frac{21}{2}El_m^2, \qquad D = 8El_m^2.$$

With these data the positive definiteness of the strain energy functional is guaranteed.

3.1. The heavy sheet problem

We consider an heavy sheet appended at the top side R and constrained at sides Q and S to have null horizontal displacement. Thus, the kinematical restrictions are

$$(\delta u_2)_R = 0, \quad (\delta u_1)_Q = 0, \quad (\delta u_1)_S = 0. \tag{39}$$

and also represented in Fig. 2. Let the two partial differential equations (6) and (7) be satisfied with the following external forces per unit area,

$$b_1^{ext} = 0, \qquad b_2^{ext} = -\rho g, \tag{40}$$

and let the edge boundary conditions be as follows,

$$u_1 = 0, \quad t_2^Q = 0, \quad \tau_1^Q = 0, \quad \tau_2^Q = \tau_2^{ext,Q}, \quad \forall X \in Q, \tag{41}$$

$$t_1^R = 0, \quad u_2 = 0, \quad \tau_1^R = 0, \quad \tau_2^R = \tau_2^{R,ext}, \quad \forall X \in R, \tag{42}$$

$$u_1 = 0, \quad t_2^S = 0, \quad \tau_1^S = 0, \quad \tau_2^S = \tau_2^{ext,S}, \quad \forall X \in S, \tag{43}$$

$$t_1^T = 0, \quad t_2^T = 0, \quad \tau_1^T = 0, \quad \tau_2^T = \tau_2^{T,ext}, \quad \forall X \in T, \tag{44}$$

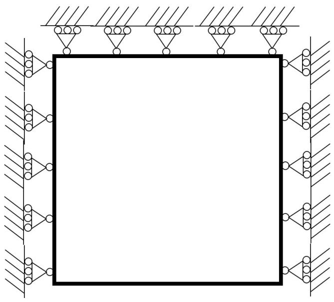

Figure 2: Graphical representation of the kinematic restrictions for the heavy sheet problem.

where the non-null external edge double forces are as follows,

$$\tau_2^{ext,Q} = \tau_2^{ext,S} = \frac{(A+B-2C)\,\rho g}{2\,(\lambda+2\mu)}, \quad \tau_2^{R,ext} = \tau_2^{T,ext} = \frac{\rho g B}{(\lambda+2\mu)}, \tag{45}$$

and let the only wedge conditions that are not implied by (41-44) be as follows,

$$\left(f_2^{ext}\right)_{V_3} = 0, \quad \left(f_2^{ext}\right)_{V_4} = 0. \tag{46}$$

The analytical solution of this problem is achieved in [61] and here represented in terms of the displacement field,

$$u_1 = 0, \qquad u_2 = \frac{\rho g\,(X_2 - l)\,(3l + X_2)}{2\,(\lambda+2\mu)}. \tag{47}$$

The numerical simulations of this problem is shown in Fig. 3a and have shown remarkable identification between exact analytical solution and the respective numerical simulation (Fig. 3b)

3.2. The bending problem

We consider the bending problem and constrain the whole side A to not displace in the horizontal direction and one of its point, the origin O, to have also null vertical displacement. Thus, the kinematical restrictions are

$$(\delta u_1)_A = 0, \quad (\delta u_2)_O = 0. \tag{48}$$

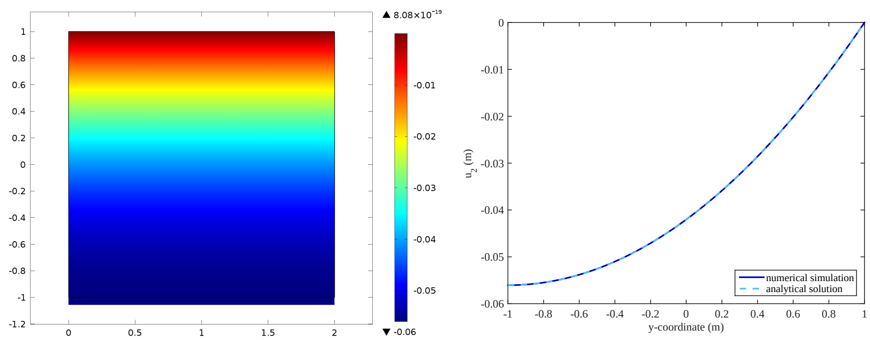

Figure 3: Vertical displacement of the heavy sheet problem. (a) Graphical representation of the numerical simulation and (b) comparison between the exact analytical solution and the respective numerical one through a given vertical cut.

and they are represented in Fig. 4. It has to be remarked that such kinematical constrains are not of a general type. In fact, the $(48)_2$ is referred to a single point that is not a vertex of the domain. This means that the results will be reasonable only in the case of vertical null force at point O. Let the two partial differential equations (6) and (7) be satisfied with the null external forces per unit area,

$$b_1^{ext} = 0, \qquad b_2^{ext} = 0, \tag{49}$$

and the edge boundary conditions be as follows,

$$u_1 = 0, \quad t_2^Q = 0, \quad \tau_1^Q = 0, \quad \tau_2^Q = \tau_2^{ext,Q}, \quad \forall X \in Q, \tag{50}$$

$$t_1^R = 0, \quad t_2^R = 0, \quad \tau_1^R = 0, \quad \tau_2^R = \tau_2^{R,ext}, \quad \forall X \in R, \tag{51}$$

$$t_1 = t_1^{ext,S}, \quad t_2^S = 0, \quad \tau_1^S = 0, \quad \tau_2^S = \tau_2^{ext,S}, \quad \forall X \in S, \tag{52}$$

$$t_1^T = 0, \quad t_2^T = 0, \quad \tau_1^T = 0, \quad \tau_2^T = \tau_2^{T,ext}, \quad \forall X \in T, \tag{53}$$

where the non-null external edge force and double forces are as follows,

$$t_1^{ext,S} = \frac{3M^{ext}X_2}{2l^3}, \tag{54}$$

$$\tau_2^{ext,Q} = \tau_2^{ext,S} = \frac{3M^{ext}\left[-\left(5\lambda + 8\mu\right)A + \left(\lambda + 4\mu\right)B + 2\lambda C - \left(4\lambda + 8\mu\right)D\right]}{16l^3\mu\left(\lambda + \mu\right)}, \tag{55}$$

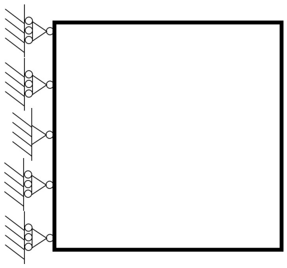

Figure 4: Graphical representation of the kinematic restrictions for the bending problem.

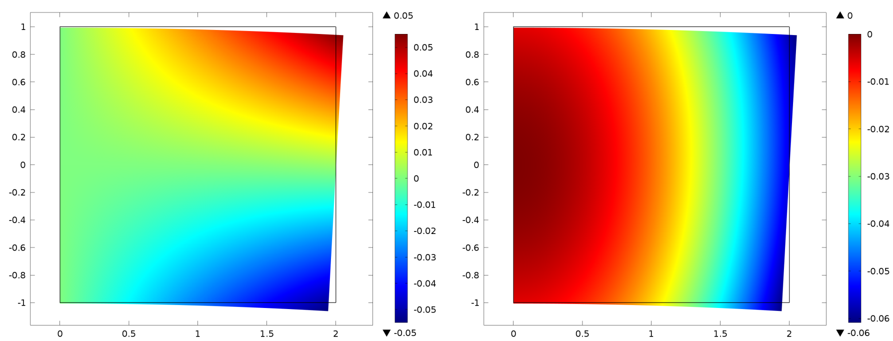

Figure 5: Numerical simulation for the bending problem. In particular, (a) horizontal and (b) vertical displacements are represented.

$$\tau_2^{R,ext} = \tau_2^{T,ext} = -\frac{3M^{ext}\left[(\lambda+2\mu)\,A + (3\lambda+2\mu)\,B - (2\lambda+4\mu)\,C - (4\lambda+8\mu)\,D\right]}{16 l^3 \mu\,(\lambda+\mu)}. \tag{56}$$

and let the only wedge conditions that are not implied by (50-53) be as follows,

$$\begin{aligned}
&\left(f_2^{ext}\right)_{V_1} = 0, \quad \left(f_2^{ext}\right)_{V_2} = 0, \quad \left(f_2^{ext}\right)_{V_3} = 0, \quad \left(f_2^{ext}\right)_{V_4} = 0,\\
&\left(f_1^{ext}\right)_{V_2} = -\left(f_1^{ext}\right)_{V_3} = \frac{3M^{ext}\left[(\lambda+2\mu)\,(A - B + 2C) + 4\mu D\right]}{8 l^3 \mu\,(\lambda+\mu)}.
\end{aligned}$$

The analytical solution of this problem is achieved in [61] and here represented in terms of the displacement field,

$$u_1 = \frac{3M^{ext}\,(\lambda+2\mu)\,X_1 X_2}{8 l^3 \mu\,(\lambda+\mu)}, \qquad u_2 = -\frac{3M^{ext}\left[\lambda X_2^2 + (\lambda+2\mu)\,X_1^2\right]}{16 l^3 \mu\,(\lambda+\mu)}, \tag{57}$$

The numerical simulations of this problem are shown in Figs. 5.

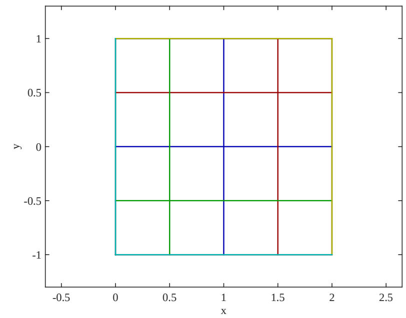

Figure 6: Horizontal and vertical cuts that are used to represent the comparison between the exact analytical and numerical simulations in Figs 7, 8, 9, 10, 13 and 14. In such figures the colors of the lines correspond to the colors of the cuts represented in this figure.

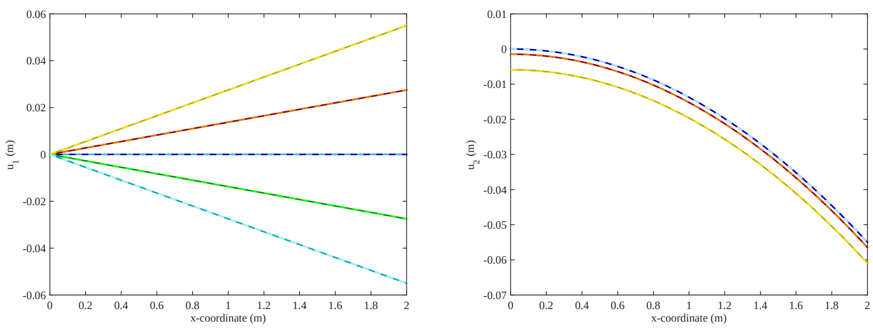

Figure 7: Comparison between the exact analytical solution and numerical simulation through the horizontal cuts of Fig. 6. In particular, (a) horizontal and (b) vertical displacements are represented.

The comparisons between the exact analytical solution and the numerical simulation have been done through the horizontal and vertical cuts of Figs. 6 and the respective numerical simulation is shown in Figs. 7 and 8.

3.3. The bending problem without double forces

We consider the same bending problem of the previous subsection, with the same kinematical restrictions (48), the same external forces per unit area (49), the same edge boundary conditions (50-53) with the same edge force (54) but with null edge double forces

$$\tau_2^{ext,Q} = \tau_2^{ext,S} = 0, \quad \tau_2^{R,ext} = \tau_2^{T,ext} = 0,$$

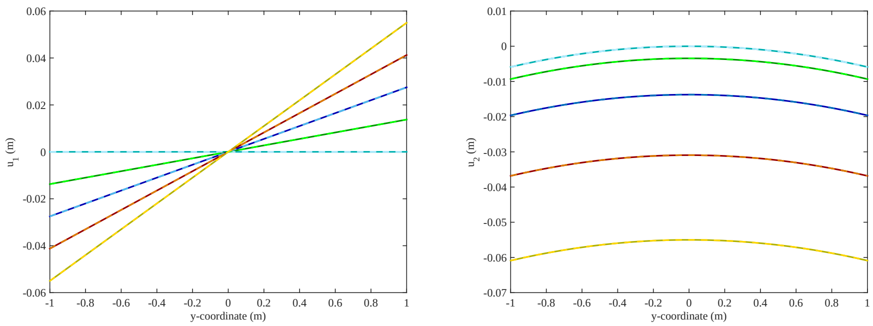

Figure 8: Comparison between the exact analytical solution and numerical simulation through the vertical cuts of Fig. 6. In particular, (a) horizontal and (b) vertical displacements are represented.

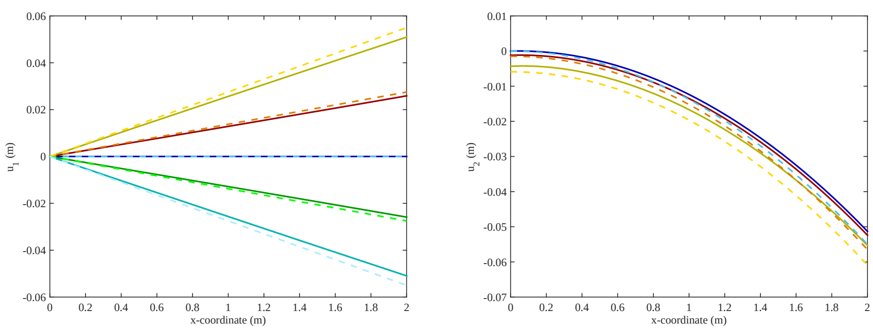

Figure 9: Comparison between the exact analytical solution with non null external double and wedge forces and numerical simulation with null external double and wedge forces through the horizontal cuts of Fig. 6. In particular, (a) horizontal and (b) vertical displacements are represented.

and null wedge conditions

$$\left(f_2^{ext}\right)_{V_1} = 0, \quad \left(f_2^{ext}\right)_{V_2} = 0, \quad \left(f_2^{ext}\right)_{V_3} = 0, \quad \left(f_2^{ext}\right)_{V_4} = 0, \left(f_1^{ext}\right)_{V_2} = -\left(f_1^{ext}\right)_{V_3} = 0.$$

In this case we do not have an analytical solution but we make numerical simulations, that are shown in Figs 9 and 10. It can be remarked that the presence of double forces has a relatively strong influence on the numerical results.

3.4. The flexure problem

We consider the flexure problem and constrain the whole side C to displace in the vertical direction and one of the point of side A, the origin O, to have null horizontal and vertical displacements.

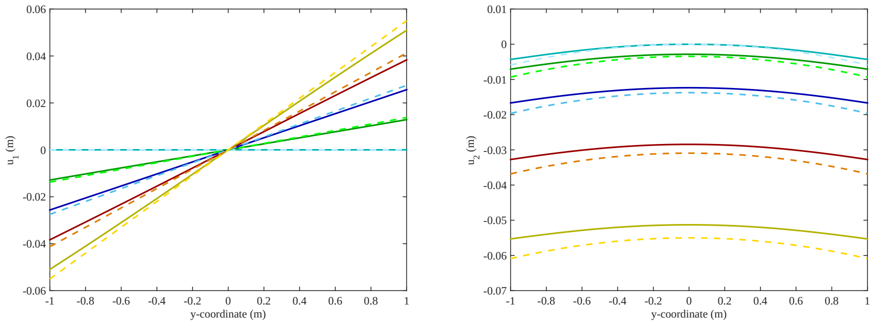

Figure 10: Comparison between the exact analytical solution with non null external double and wedge forces and numerical simulation with null external double and wedge forces through the vertical cuts of Fig. 6. In particular, (a) horizontal and (b) vertical displacements are represented.

Thus, the kinematical restrictions are

$$(\delta u_1)_S = 0, \quad (\delta u_1)_O = 0 \quad (\delta u_2)_O = 0. \tag{58}$$

and they are represented in Fig. 11. It has to be remarked that such kinematical constrain are not of a general type. In fact, the $(58)_{2,3}$ is referred to a single point that is not a vertex of the domain. This means that the results will be reasonable only in the case of null force at point O. Let the two partial differential equations (6) and (7) be satisfied with null external forces per unit area (49), let the edge boundary conditions be as follows,

$$t_1 = t_1^{ext,Q}, \quad t_2^Q = t_2^{ext,Q}, \quad \tau_1^Q = \tau_1^{ext,Q}, \quad \tau_2^Q = \tau_2^{ext,Q}, \quad \forall X \in Q, \tag{59}$$

$$t_1 = t_1^{ext,R}, \quad t_2^R = 0, \quad \tau_1^R = \tau_1^{ext,R}, \quad \tau_2^R = \tau_2^{R,ext}, \quad \forall X \in R, \tag{60}$$

$$t_1 = 0, \quad u_2 = -\delta, \quad \tau_1^S = \tau_1^{ext,S}, \quad \tau_2^S = 0, \quad \forall X \in S, \tag{61}$$

$$t_1 = t_1^{ext,T}, \quad t_2^T = 0, \quad \tau_1^T = \tau_1^{ext,T}, \quad \tau_2^T = \tau_2^{T,ext}, \quad \forall X \in T, \tag{62}$$

where the non-null external edge force and double forces are as follows,

$$t_1^{ext,Q} = -\frac{3LQX_2}{2l^3} \tag{63}$$

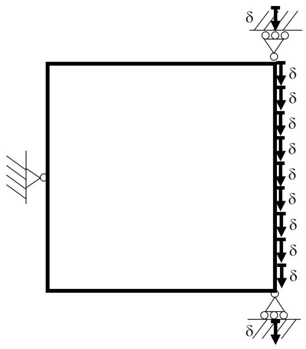

Figure 11: Graphical representation of the kinematic restrictions for the flexure problem.

$$t_2^{ext,Q} = \frac{3Q\left[-A\lambda + B\left(5\lambda+4\mu\right) + 2C\lambda - 4D\left(3\lambda+4\mu\right) + 4\mu\lambda\left(l^2 - X_2^2\right) + 4\mu^2\left(l^2 - X_2^2\right)\right]}{16l^3\mu\left(\lambda+\mu\right)} \tag{64}$$

$$t_1^{ext,R} = -t_1^{ext,T} = -\frac{3Q}{16l^3\mu\left(\lambda+\mu\right)}\left[\left(\lambda+2\mu\right)\left(A-2C-4D\right) + B\left(3\lambda+2\mu\right)\right] \tag{65}$$

$$t_1^{ext,S} = \frac{3M^{ext}X_2}{2l^3}, \tag{66}$$

$$\tau_1^{ext,Q} = \tau_1^{ext,S} = \frac{3QX_2\left[\left(3\lambda+4\mu\right)\left(A-2C\right) + \lambda\left(B+4D\right)\right]}{16l^3\mu\left(\lambda+\mu\right)}. \tag{67}$$

$$\tau_2^{ext,Q} = -\frac{3QL\left[\left(5\lambda+8\mu\right)A - \left(\lambda+4\mu\right)B - 2\lambda C + \left(\lambda+2\mu\right)4D\right]}{16l^3\mu\left(\lambda+\mu\right)}, \tag{68}$$

$$\tau_1^{ext,R} = -\tau_1^{ext,T} = \frac{3Q\left[\left(\lambda+2\mu\right)\left(3A+2C\right) + \left(\lambda-2\mu\right)B - 4\lambda D\right]}{16l^2\mu\left(\lambda+\mu\right)} \tag{69}$$

$$\tau_2^{ext,R} = \tau_2^{ext,T} = -\frac{3Q\left(L-X_1\right)\left[\left(\lambda+2\mu\right)\left(A-2C-4D\right) + \left(3\lambda+2\mu\right)B\right]}{16l^3\mu\left(\lambda+\mu\right)}, \tag{70}$$

and the only wedge conditions that are not implied by (59-62) are as follows,

$$\begin{aligned}
&\left(f_1^{ext}\right)_{V_1} = -\left(f_1^{ext}\right)_{V_4} = -\frac{3QL\left[\left(\lambda+2\mu\right)\left(A-B+2C\right) + 4\mu D\right]}{8l^3\mu\left(\lambda+\mu\right)},\\
&\left(f_2^{ext}\right)_{V_1} = \left(f_2^{ext}\right)_{V_4} = \frac{3Q\left[\left(3\lambda+4\mu\right)\left(A-B\right) - 2\lambda C + 4\left(2\lambda+3\mu\right)D\right]}{8l^2\mu\left(\lambda+\mu\right)},\\
&\left(f_1^{ext}\right)_{V_2} = 0, \quad \left(f_1^{ext}\right)_{V_3} = 0.
\end{aligned}$$

The analytical solution of this problem is achieved in [61] and here represented in terms of the

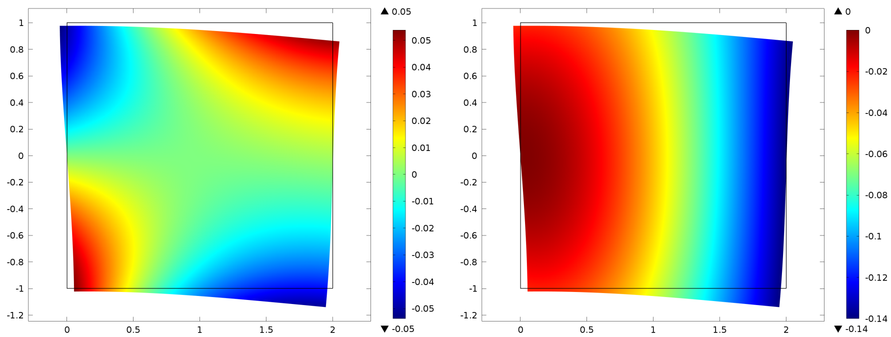

Figure 12: Numerical simulation for the flexure problem. In particular, (a) horizontal and (b) vertical displacements are represented.

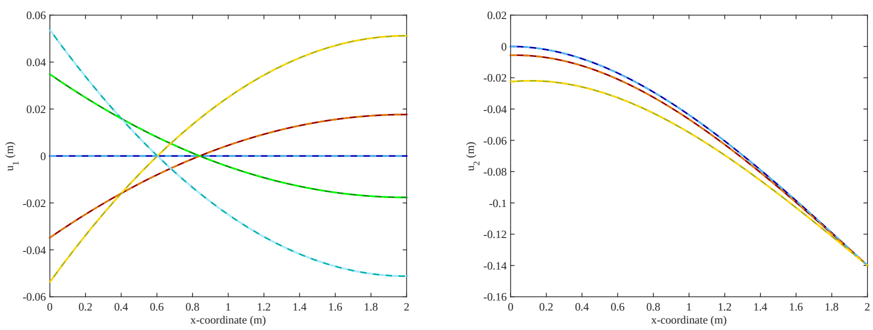

Figure 13: Comparison between the exact analytical solution and numerical simulation through the horizontal cuts of Fig. 6a. In particular, (a) horizontal and (b) vertical displacements are represented.

displacement field,

$$u_1 = -\frac{QX_2\left[(\lambda+2\mu)\left(3X_1^2 - X_2^2 - 6LX_1\right) + 2\left(\lambda+\mu\right)\left(6l^2 - X_2^2\right)\right]}{16l^3\mu\left(\lambda+\mu\right)}, \tag{71}$$

$$u_2 = -\frac{Q\left[(3L - X_1)\left(\lambda+2\mu\right)X_1^2 + 3\left(L - X_1\right)\lambda X_2^2\right]}{16l^3\mu\left(\lambda+\mu\right)}, \tag{72}$$

The numerical simulations of this problem are shown in Figs. 12.

The comparisons between the exact analytical solution and the numerical simulation have been done through the horizontal and vertical cuts of Figs. 6 and the respective numerical simulation is shown in Figs. 13 and 14.

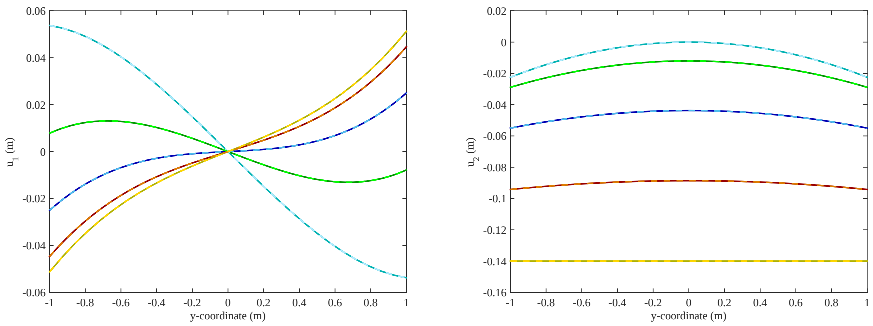

Figure 14: Comparison between the exact analytical solution and numerical simulation through the vertical cuts of Fig. 6b. In particular, (a) horizontal and (b) vertical displacements are represented.

3.5. Convergence analysis for the wedge force problem

We consider again the bending problem with the same kinematical restrictions (48) (see also Fig. 4), the same external forces per unit area (49), the same edge boundary conditions (50-53) but with null edge forces and double forces at side C as follows,

$$t_1^{ext,S} = 0, \quad \tau_2^{ext,Q} = \tau_2^{ext,S} = 0, \quad \tau_2^{R,ext} = \tau_2^{T,ext} = 0,$$

and with the following system of wedge conditions

$$\left(f_2^{ext}\right)_{V_1} = 0, \quad \left(f_2^{ext}\right)_{V_2} = 0, \quad \left(f_2^{ext}\right)_{V_3} = -F, \quad \left(f_2^{ext}\right)_{V_4} = 0, \quad \left(f_1^{ext}\right)_{V_2} = -\left(f_1^{ext}\right)_{V_3} = 0.$$

Even in this modified bending case we do not have an analytical solution but we make numerical simulations, that are shown in Figs 15. On the left-hand side we show the results of a numerical simulation of the analogous problem in the classical first gradient model and on the right-hand side a the results of a numerical simulation with the present second gradient model.

It is immediately visible from Fig. 15 that the first gradient model is not adequate for wedge concentrated external forces. In Fig. 16 a convergence analysis is performed. From such a convergence analysis we deduce that first gradient models are not adequate to model concentrated external forces.

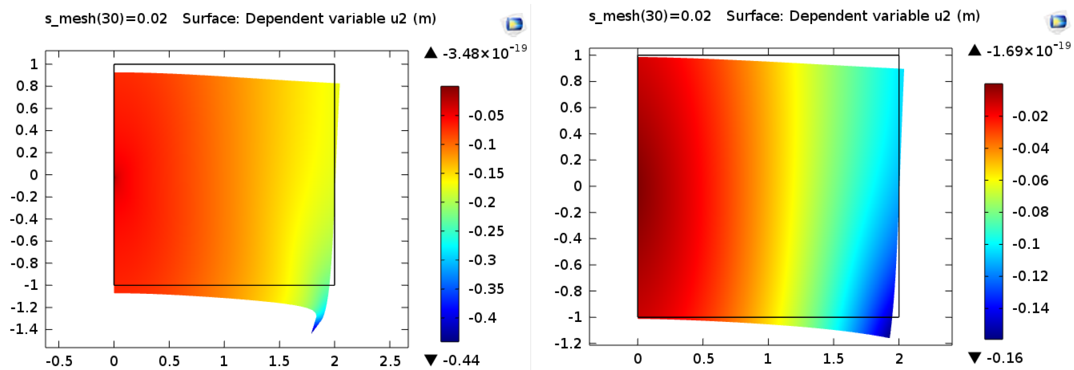

Figure 15: Comparison between the vertical displacement in the (a) first and (b) second gradient models in the case of an external wedge force.

4. Experimental evidence of elastic second gradient contribution to the deformation energy

In [31] it is shown that second-gradient energy terms allow the onset of internal shear boundary layers. These boundary layers are transition zones between two different shear deformation modes. In the same paper, on the one hand it is claimed that their existence cannot be described by a simple first-gradient model, and on the other hand that they are related to second-gradient material coefficients. In this section we show a result, on the pantographic structure of Fig. 17, that makes explicit the experimental evidence of such a boundary layer. Besides, by using the second gradient model of [25], we show that it is possible to characterize the largeness of the boundary layer in terms of the second gradient coefficient (i.e., K_{II}) of that model, that means that a simple first gradient model (i.e., a model with $K_{II}=0$) is not sufficient to predict the correct experimental evidence.

The elastic non-linear anisotropic internal energy density of the model that is used in [25] to numerically evaluate the shear angles that are shown in Fig. 18 is the following,

$$U\left(F,\nabla F\right)=\sum_{\alpha=1}^{2}\{\frac{K_e}{2}\left(F_{ab}D_b^\alpha-1\right)\left(F_{ac}D_c^\alpha-1\right) \tag{73}$$
$$+\frac{K_{II}}{2}\left[\frac{F_{ab,c}F_{ad,e}D_b^\alpha D_c^\alpha D_d^\alpha D_e^\alpha}{F_{fg}F_{fh}D_g^\alpha D_h^\alpha}-\left(\frac{F_{ab}F_{ac,d}D_b^\alpha D_c^\alpha D_d^\alpha}{F_{fg}F_{fh}D_g^\alpha D_h^\alpha}\right)^2\right]\}$$

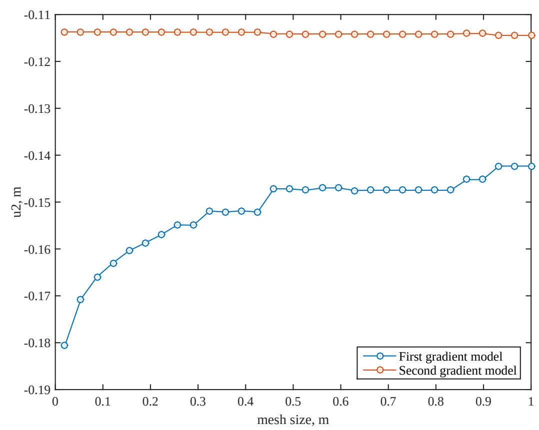

Figure 16: Comparison between the vertical displacement at the center of side S in the (a) first and (b) second gradient models in the case of an external vertical wedge force at V_3.

$$+\frac{K_b}{2}\left[\arccos\frac{F_{ab}F_{ac}D_b^1D_c^2}{\sqrt{F_{de}F_{df}D_e^1D_f^1}\sqrt{F_{gh}F_{gi}D_h^2D_i^2}}-\frac{\pi}{2}\right]^{\gamma}$$

where the two families of fibers are initially directed along the two orthogonal unit vectors $\mathbf{D}^1$ and$\mathbf{D}^2$and where the material coefficients that have been used are $K_e = 0.134\,MN/m$, $K_p = 159\,N/m$ and $\gamma = 1.36$. We also remark that the bias test that is shown in Fig. 17 is accomplished by imposing a displacement, towards the direction parallel to the long side of the rectangle, of the short-side of the rectangle, that in turn is directed at $\pi/4$ with respect to the two orthogonal unit vectors $\mathbf{D}^1$ and$\mathbf{D}^2$. In the deformed configuration the angle φ between the two families of fibers is not anymore at $\pi/2$. It is

$$\varphi = \arccos\frac{F_{ab}F_{ac}D_b^1D_c^2}{\sqrt{F_{de}F_{df}D_e^1D_f^1}\sqrt{F_{gh}F_{gi}D_h^2D_i^2}},$$

and the shear angle ϕ (or shear deformation in Fig. 18) is simply

$$\phi = \varphi - \frac{\pi}{2}.$$

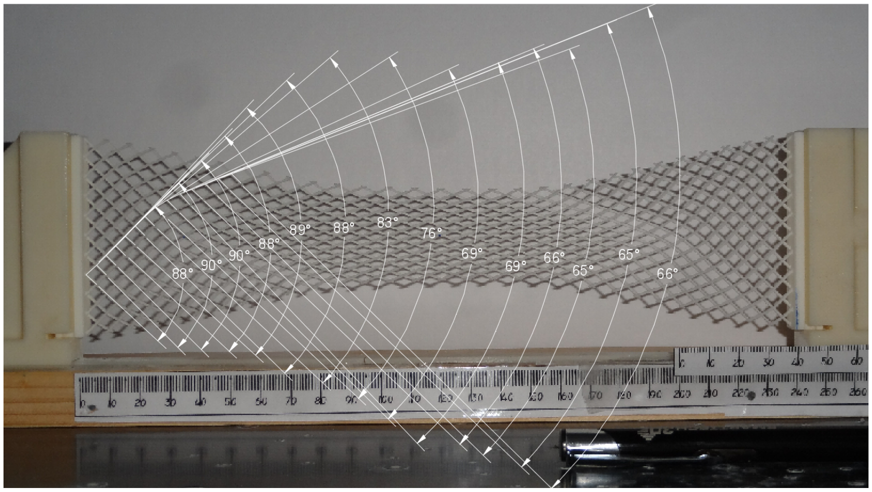

Figure 17: A bias test on a standard pantographic structure is shown. The angles across the two families of fibers in the deformed configuration are evaluated by image analysis.

If we evaluate the shear angle ϕ along the arc-length that is shown in Fig. 17, it is almost zero near short side of the rectangle and reach a finite value by passing through a boundary layer. The largeness of such a boundary layer is related to the second gradient parameter K_{II}.

In Fig. 18 we show that the optimal value for the second gradient constitutive parameter K_{II} is $K_{II} = 0.0192\,Nm$. However, we also shown that different values of this parameter give a wrong largeness of the boundary layer. In particular we observe that a reduction 1/4 of the second gradient constitutive parameter K_{II} give a smaller boundary layer and a magnification of 4 give a larger boundary layer. Finally, a numerical simulation in which the second gradient contribution of the strain energy (73) is assumed to vanish, i.e. $K_{II} = 0$, produce no-boundary layer. Besides, numerically instability is observed in this last case.

5. Conclusions

A perfect overlap of numerical simulations obtained with a commercial code and closed form solution of selected classical benchmark boundary value problems have bee found and reported in this paper. The role of external double and wedge forces has also been presented. Besides, we show a mesh-independent behaviour of second gradient numerical solution with respect to the correspond-

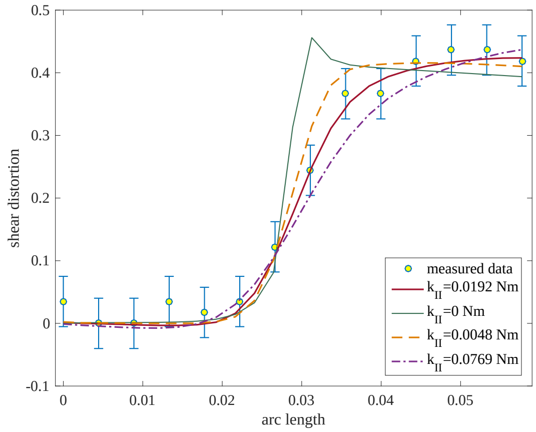

Figure 18: The boundary layer of the case related to the experiment that is shown in Fig. 17 is shown. The angles across the two families of fibers in the deformed configuration are evaluated by image analysis of the experimental result of Fig. 17 and by numerical simulations with different values of second gradient coefficients K_{II}.

ing first gradient counterpart. Finally, we show an experimental bias test on a specific pantographic structure and extrapolate an internal boundary layer in terms of the shear angles across initially orthogonal fibers. A non-linear anisotropic model is also presented aimed to reproduce the shown experimental results. In particular, we exhibit comparisons between the numerical simulation of the proposed theoretical model and the experimental results in terms of the internal boundary layer. Such a comparison has permitted to identify the second gradient coefficient of this model.

References

[1] Akarapu S, Zbib HM. Numerical analysis of plane cracks in strain-gradient elastic materials. International Journal of Fracture 2006; 141(3–4):403–430. DOI: 10.1007/s10704-006-9004-y.

[2] Alibert, Jean-Jacques, and Alessandro Della Corte. "Second-gradient continua as homogenized limit of pantographic microstructured plates: a rigorous proof." Zeitschrift für angewandte Mathematik und Physik 66.5 (2015): 2855-2870.

[3] Altenbach, H., Eremeyev, V.A., Morozov, N.F., On equations of the linear theory of shells with surface stresses taken into account, Mechanics of Solids, 45 (3), pp. 331-342 (2010)

[4] D. Assante, C. Cesarano, Simple semi-analytical expression of the lightning base current in the frequency-domain, Journal of Engineering Science and Technology Review, 7 (2), pp. 1-6 (2014)

[5] Atluri, S.N., Cazzani, A., Rotations in computational solid mechanics, Archives of Computational Methods in Engineering, Volume 2, Issue 1, March 1995, Pages 49-138

[6] Aminpour, H., Rizzi, N. A one-dimensional continuum with microstructure for single-wall carbon nanotubes bifurcation analysis. Mathematics and Mechanics of Solids. Volume 21, Issue 2, 1 February 2016, Pages 168-181.

[7] Aminpour, H., Rizzi, N. On the continuum modelling of carbon nano tubes. Civil-Comp Proceedings Volume 108, 2015

[8] Aminpour, H., Rizzi, N. On the modelling of carbon nano tubes as generalized continua. Advanced Structured Materials. Volume 42, 1 April 2016, Pages 15-35.

[9] Aminpour, H., Rizzi, N., Salerno, G. A one-dimensional beam model for single-wall carbon nano tube column buckling. Civil-Comp Proceedings. Volume 106, 2014.

[10] Andreaus, U., Giorgio, I., Lekszycki, T., A 2-D continuum model of a mixture of bone tissue and bio-resorbable material for simulating mass density redistribution under load slowly variable in time, ZAMM Zeitschrift fur Angewandte Mathematik und Mechanik, Volume 94, Issue 12, 1 December 2014, Pages 978-1000

[11] Argyris J.H., Fried I., Scharpf D.W., The TUBA family of plate elements for the matrix displacement method. Aeronautical Journal of the Royal Aeronautical Society 1968; 72(692):701–709.

[12] Auffray, N., dell'Isola, F., Eremeyev, V.A., Madeo, A., Rosi, G., Analytical continuum mechanics à la Hamilton-Piola least action principle for second gradient continua and capillary fluids, Mathematics and Mechanics of Solids, Volume 20, Issue 4, 4 April 2015, Pages 375-417

[13] Auffray, Nicolas, Regis Bouchet, and Yves Brechet. "Derivation of anisotropic matrix for bi-dimensional strain-gradient elasticity behavior." International Journal of Solids and Structures 46.2 (2009): 440-454.

[14] Bilotta, A., Formica, G., Turco, E., Performance of a high-continuity finite element in three-dimensional elasticity, International Journal for Numerical Methods in Biomedical Engineering, Volume 26, Issue 9, September 2010, Pages 1155-1175

[15] Bilotta, A., Turco, E., A numerical study on the solution of the Cauchy problem in elasticity, International Journal of Solids and Structures, 46 (25-26), pp. 4451-4477, (2009)

[16] Bulíček, M., Málek, J., Rajagopal, K. R., & Walton, J. R. (2015). Existence of solutions for the anti-plane stress for a new class of "strain-limiting" elastic bodies. Calculus of Variations and Partial Differential Equations, 54(2), 2115-2147

[17] Carcaterra, A., Roveri, N., Energy distribution in impulsively excited structures, Shock and Vibration, Volume 19, Issue 5, 2012, Pages 1143-1163

[18] C. Cesarano, Generalized Chebyshev polynomials, Hacettepe Journal of Mathematics and Statistics, 43 (5), pp. 731-740 (2014)

[19] Cesarano, C., Assante, D. A note on generalized Bessel functions, International Journal of Mathematical Models and Methods in Applied Sciences, 8 (1), pp. 38-42 (2014)

[20] Cesarano, C., Fornaro, C., Vazquez, L., Operational results on bi-orthogonal hermite functions, Acta Mathematica Universitatis Comenianae, 85 (1), pp. 43-68 (2016)

[21] Cuomo, M., Contrafatto, L., Greco, L., A variational model based on isogeometric interpolation for the analysis of cracked bodies, International Journal of Engineering Science, Volume 80, July 2014, Pages 173-188

[22] Dasgupta S, Sengupta D. A higher-order triangular plate bending element revisited. International Journal for Numerical Methods in Engineering 1990; 30:419–430. DOI: 10.1002/nme.1620300303.

[23] de Oliveira Góes, R. C., de Castro, J. T. P. and Martha, L. F.. 3D effects around notch and crack tips. International Journal of Fatigue, 62, 159-170, 2014.

[24] Del Vescovo, D., Giorgio, I., Dynamic problems for metamaterials: Review of existing models and ideas for further research, International Journal of Engineering Science 80, pp. 153-172 (2014)

[25] dell'Isola, F., Giorgio, I., Pawlikowski, M., Rizzi, N.L. Large deformations of planar extensible beams and pantographic lattices: Heuristic homogenization, experimental and numerical examples of equilibrium. Proceedings of the Royal Society A: Mathematical, Physical and Engineering Sciences. Volume 472, Issue 2185, 2016, Article number 20150790 pages (23)

[26] F. dell'Isola, M. Guarascio, and K. Hutter, "A variational approach for the deformation of a saturated porous solid. A second-gradient theory extending Terzaghi's effective stress principle", Archive of Applied Mechanics, vol. 70 (5), 2000, pp. 323-337.

[27] F. dell'Isola, A. Madeo and L. Placidi "Linear plane wave propagation and normal transmission and reflection at discontinuity surfaces in second gradient 3D Continua", ZAMM – Journal of Applied Mathematics and Mechanics / Zeitschrift für Angewandte Mathematik und Mechanik, vol. 92 (1), 2012, pp. 52-71.

[28] S. Federico, Grillo A., W. Herzog, A Transversely Isotropic Composite with a Statistical Distribution of Spheroidal Inclusions: a Geometrical Approach to Overall Properties, Journal of the Mechanics and Physics of Solids, 2004, volume 52, pages 2309-2327

[29] S. Federico, A. Grillo, S. Imatani, The Linear Elasticity Tensor of Incompressible Materials, Mathematics and Mechanics of Solids, 2014, in press, DOI: 10.1177/1081286514550576.

[30] S. Federico, A. Grillo, G. Wittum, Considerations on Incompressibility in Linear Elasticity, Nuovo Cimento C, 2009, 32C, pages 81-87.

[31] M. Ferretti, A. Madeo, F. dell'Isola and P. Boisse "Modelling the onset of shear boundary

layers in fibrous composite reinforcements by second gradient theory", ZAMP – Zeitschrift für angewandte Mathematik und Physik, vol. 65 (3), 2014, pp. 587-612.

[32] Fischer, P., Klassen, M., Mergheim, J., Steinmann, P., Müller, R., Isogeometric analysis of 2D gradient elasticity, Computational Mechanics, 47:325–334 (2011)

[33] Fischer P, Mergheim J, Steinmann P. On the C1 continuous discretization of non-linear gradient elasticity: a comparison of NEM and FEM based on Bernstein–Bézier patches. International Journal for Numerical Methods in Engineering 2010; 82(10):1282–1307. DOI: 10.1002/nme.2802.

[34] Gabriele, S., Rizzi, N., Varano, V. A 1D nonlinear TWB model accounting for in plane cross-section deformation. International Journal of Solids and Structures. 2016, 94-95, 170-178.

[35] Gabriele, S., Rizzi, N.L., Varano, V. A one-dimensional nonlinear thin walled beam model derived from Koiter shell theory. Civil-Comp Proceedings Volume 106, 2014.

[36] Gabriele, S., Rizzi, N., Varano, V. On the imperfection sensitivity of thin-walled frames. Civil-Comp Proceedings .Volume 99, 2012 11th International Conference on Computational Structures Technology, CST 2012; Dubrovnik; Croatia; 4 September 2012 through 7 September 2012; Code 102644

[37] Garusi, E., Tralli, A., Cazzani, A., An unsymmetric stress formulation for Reissner-Mindlin plates: A simple and locking-free rectangular element, International Journal of Computational Engineering Science, 5 (3), pp. 589-618 (2004)

[38] Ghiba Ionel-Dumitrel, Neff Patrizio, Madeo Angela, Placidi L, Rosi Giuseppe (2015). The relaxed linear micromorphic continuum: existance, uniqueness and continuous dependence in dynamics. MATHEMATICS AND MECHANICS OF SOLIDS, vol. 20, p. 1171-1197, ISSN: 1081-2865, doi: 10.1177/1081286513516972.

[39] Greco, L., & Cuomo, M. (2015). Consistent tangent operator for an exact Kirchhoff rod model. Continuum Mechanics and Thermodynamics, 27(4-5), 861-877.

[40] R. Hill, A Self-Consistent Mechanics of Composite Materials, Journal of the Mechanics and Physics of Solids, 1965, 13, pages 213-222.

[41] Javili, A., Dell'Isola, F., Steinmann, P., Geometrically nonlinear higher-gradient elasticity with energetic boundaries, Journal of the Mechanics and Physics of Solids 61 (12), pp. 2381-2401, (2013)

[42] A. Madeo, F. dell'Isola and F. Darve "A continuum model for deformable, second gradient porous media partially saturated with compressible fluids", Journal of the Mechanics and Physics of Solids, vol. 61 (11), 2013, pp. 2196-2211.

[43] A. Madeo, P. Neff, I.-D. Ghiba, Placidi L, G. Rosi (2015). Band gaps in the relaxed linear micromorphic continuum. ZEITSCHRIFT FÜR ANGEWANDTE MATHEMATIK UND MECHANIK, vol. 95, p. 880-887, ISSN: 1521-4001, doi: 10.1002/zamm.201400036.

[44] Angela Madeo, Patrizio Neff, Ionel-Dumitrel Ghiba, Placidi L, Giuseppe Rosi (2015). Wave propagation in relaxed micromorphic continua: modelling metamaterials with frequency band-gaps. CONTINUUM MECHANICS AND THERMODYNAMICS, vol. 27, p. 551-570, ISSN: 0935-1175, doi: 10.1007/s00161-013-0329-2.

[45] Mareno, Anita, and Timothy J. Healey. "Global continuation in second-gradient nonlinear elasticity." SIAM journal on mathematical analysis 38.1 (2006): 103-115.

[46] Milton, G., Seppecher, P., A metamaterial having a frequency dependent elasticity tensor and a zero effective mass density, Physica Status Solidi (B) Basic Research, Volume 249, Issue 7, July 2012, Pages 1412-1414.

[47] Mindlin, R. D. (1936). Force at a point in the interior of a semi-infinite solid. Journal of Applied Physics, 7(5), 195-202.

[48] R. D. Mindlin, Micro-structure in Linear Elasticity, Department of Civil Engineering Columbia University New York 27, New York, 1964.

[49] Misra, A., Parthasarathy, R., Singh, V., Spencer, P., Micro-poromechanics model of fluid-saturated chemically active fibrous media, ZAMM Zeitschrift fur Angewandte Mathematik und Mechanik, Volume 95, Issue 2, 1 February 2015, Pages 215-234

[50] Misra, A., Singh, V., Nonlinear granular micromechanics model for multi-axial rate-dependent behavior, International Journal of Solids and Structures, Volume 51, Issue 13, 15 June 2014, Pages 2272-2282

[51] Patrizio Neff, Ionel-Dumitrel Ghiba, Angela Madeo, Placidi L, Giuseppe Rosi (2014). A unifying perspective: the relaxed linear micromorphic continuum. Continuum Mechanics and Thermodynamics, vol. 26, p. 639-681, ISSN: 0935-1175, doi: 10.1007/s00161-013-0322-9.

[52] Neff, P., Jeong, J. and Ramézani, H. Subgrid interaction and micro-randomness–Novel invariance requirements in infinitesimal gradient elasticity. International Journal of Solids and Structures, 46(25), 2009, 4261-4276.

[53] Papanicolopulos, S.-A., Zervos, A. A method for creating a class of triangular C 1 finite elements (2012) International Journal for Numerical Methods in Engineering, 89 (11), pp. 1437-1450.

[54] Papanicolopulos, S.-A., Zervos, A., Vardoulakis, I. A three-dimensional C1 finite element for gradient elasticity (2009) International Journal for Numerical Methods in Engineering, 77 (10), pp. 1396-1415.

[55] Piccardo, G., Ranzi, G., Luongo, A., A complete dynamic approach to the Generalized Beam Theory cross-section analysis including extension and shear modes, Mathematics and Mechanics of Solids, 19 (8), pp. 900-924 (2014)

[56] Piccardo, G., Ranzi, G., Luongo, A., A direct approach for the evaluation of the conventional modes within the GBT formulation, Thin-Walled Structures, Volume 74, 2014, Pages 133-145

[57] Pideri, Catherine, and Pierre Seppecher. "A second gradient material resulting from the ho-

mogenization of an heterogeneous linear elastic medium." Continuum Mechanics and Thermodynamics 9.5 (1997): 241-257.

[58] Pignataro, M., Ruta, G., Rizzi, N., Varano, V. Effects of warping constraints and lateral restraint on the buckling of thin-walled frames. ASME International Mechanical Engineering Congress and Exposition, Proceedings Volume 10, Issue PART B, 2010, Pages 803-810. ASME 2009 International Mechanical Engineering Congress and Exposition, IMECE2009; Lake Buena Vista, FL; United States; 13 November 2009 through 19 November 2009; Code 80879

[59] Placidi Luca (2016). A variational approach for a nonlinear one-dimensional damage-elasto-plastic second-gradient continuum model. CONTINUUM MECHANICS AND THERMODYNAMICS, vol. 28, p. 119-137, ISSN: 0935-1175, doi: 10.1007/s00161-014-0405-2.

[60] Placidi Luca (2015). A variational approach for a nonlinear 1-dimensional second gradient continuum damage model. CONTINUUM MECHANICS AND THERMODYNAMICS, vol. 27, p. 623-638, ISSN: 0935-1175, doi: 10.1007/s00161-14-0338-9.

[61] Placidi Luca, Ugo Andreaus, Alessandro Della Corte, Tomasz Lekszycki (2015). Gedanken experiments for the determination of two-dimensional linear second gradient elasticity coefficients. ZEITSCHRIFT FUR ANGEWANDTE MATHEMATIK UND PHYSIK, vol. 66, p. 3699-3725, ISSN: 0044-2275, doi: 10.1007/s00033-015-0588-9.

[62] Placidi L, Andreaus U., Giorgio I. (in press). Identification of two-dimensional pantographic structure via a linear D4 orthotropic second gradient elastic model. JOURNAL OF ENGINEERING MATHEMATICS, ISSN: 0022-0833, doi: 10.1007/s10665-016-9856-8

[63] Rizzi, N.L., Varano, V. On the postbuckling analysis of thin-walled frames. Proceedings of the 13th International Conference on Civil, Structural and Environmental Engineering Computing. 2011, 14p 13th International Conference on Civil, Structural and Environmental Engineering Computing, CC 2011; Chania, Crete; Greece; 6 September 2011 through 9 September 2011; Code 89029

[64] Rosi, G., Giorgio, I., Eremeyev, V.A., Propagation of linear compression waves through plane interfacial layers and mass adsorption in second gradient fluids, ZAMM Zeitschrift fur Angewandte Mathematik und Mechanik, 93 (12), pp. 914-927 (2013)

[65] Roveri, N., Carcaterra, A., Akay, A., Vibration absorption using non-dissipative complex attachments with impacts and parametric stiffness, Journal of the Acoustical Society of America, 126 (5), pp. 2306-2314, (2009)

[66] Sansour, C. and Skatulla, S., A strain gradient generalized continuum approach for modelling elastic scale effects. Computer Methods in Applied Mechanics and Engineering, 198(15), 2009, 1401-1412.

[67] Scerrato, D., Giorgio, I., Rizzi, N.L. Three-dimensional instabilities of pantographic sheets with parabolic lattices: numerical investigations. Zeitschrift fur Angewandte Mathematik und Physik Volume 67, Issue 3, 1 June 2016, Article number 53.

[68] Scerrato, D., Zhurba Eremeeva, I.A., Lekszycki, T., Rizzi, N.L. On the effect of shear stiffness on the plane deformation of linear second gradient pantographic sheets. ZAMM Zeitschrift fur Angewandte Mathematik und Mechanik. 2016. DOI: 10.1002/zamm.201600066

[69] G. Sciarra, F. dell'Isola, and O. Coussy, Second gradient poromechanics, International Journal of Solids and Structures, vol. 44 (20), 2007, p. 6607–6629.

[70] P. Seppecher, J.-J. Alibert and F. dell'Isola, Linear elastic trusses leading to continua with exotic mechanical interactions, Journal of Physics: Conference Series vol. 319 (1), 2011, 13 pages.

[71] Terravecchia, S., Panzeca, T. and Polizzotto, C. Strain gradient elasticity within the symmetric BEM formulation. Fracture and Structural Integrity, (29), 2014, 61-73.

[72] L. J. Walpole, Elastic Behavior of Composite Materials: Theoretical Foundations, Advances in Mechanics, 1981, 21, PAGES 169-242.

[73] L. J. Walpole, Fourth-Rank Tensors of the Thirty-Two Crystal Classes: Multiplication Tables, Proceedings of the Royal Society of London Series A, 1984, 391, PAGES 149-179.

[74] Yang, Y., Misra, A., Micromechanics based second gradient continuum theory for shear band modeling in cohesive granular materials following damage elasticity, International Journal of Solids and Structures, 49 (18), pp. 2500-2514 (2012)

[75] Zervos, A. Finite elements for elasticity with microstructure and gradient elasticity (2008) International Journal for Numerical Methods in Engineering, 73 (4), pp. 564-595.

[76] Zervos, A., Papanastasiou, P., Cook, J. Elastoplastic finite element analysis of inclined wellbores (1998) Proceedings of the SPE/ISRM Rock Mechanics in Petroleum Engineering Conference, 1, pp. 535-544.

[77] Zervos, A., Papanastasiou, P., Vardoulakis, I. A finite element displacement formulation for gradient elastoplasticity (2001) International Journal for Numerical Methods in Engineering, 50 (6), pp. 1369-1388.

[78] Zervos A, Papanicolopulos SA, Vardoulakis I (2009) Two finite element discretizations for gradient elasticity. J Eng Mech 13(3):203–213 DOI: 10.1061/(ASCE)0733-9399(2009)135:3(203)

[79] Zhang, H., Wu, J., Zheng, Y., An adaptive multiscale method for strain localization analysis of 2D periodic lattice truss materials, Philosophical Magazine, 92:28-30, 3723-3752 (2012)